Hypomethylating agents induce epigenetic and transcriptional heterogeneity with implications for AML cell self-renewal

Danielle R Bond[1,2^*], Sean M Burnard[1,2^], Kumar Uddipto[1,2], Kooper V Hunt[1,2], Brooke M Harvey[1,2], Luiza Steffens Reinhardt[1,3,9], Charley Lawlor-O'Neill[1], Ellise A Roper[1], Sam Humphries[1,2], Heather C. Murray[1,2], Abdul Mannan[1,2], Matthew D Dun[1,2], Charles E de Bock[4,5], Nikola A Bowden[6,7], Anoop K Enjeti[2,6,8,9], Nicole M Verrills[1,2], Carlos Riveros[6], Kim-Anh Lê Cao[10], Heather J Lee[1,2*]

[1]*School of Biomedical Science and Pharmacy, The University of Newcastle, Australia.*

[2]*Precision Medicine Research Program, Hunter Medical Research Institute, Australia.*

[3]*Cancer Detection and Therapy Research Program, Hunter Medical Research Institute, Australia.*

[4]*Children's Cancer Institute, Lowy Cancer Research Centre, Randwick, NSW 2031, Australia*

[5]*School of Clinical Medicine, Faculty of Medicine, UNSW Sydney, NSW 2052, Australia*

[6]*School of Medicine and Public Health, The University of Newcastle, Australia.*

[7]*Drug Repurposing and Medicines Program, Hunter Medical Research Institute, Australia.*

[8]*Department of Haematology, Calvary Mater Hospital, Australia.*

[9]*New South Wales Health Pathology, John Hunter Hospital, Australia.*

[10]*Melbourne Integrative Genomics, School of Mathematics and Statistics, The University of Melbourne, Australia.*

^ These authors contributed equally to this work; * Corresponding authors

Correspondence should be directed to A/Prof Heather J Lee: Heather.lee@newcastle.edu.au

Competing Interests

A.K.E. declares the following competing interests: advisory board and honoraria from AbbVie, Astellas, Gilead, Servier, Jazz, Otsuka/Astex, and RACE Oncology; speaker fees from AbbVie,

Otsuka/Astex, Astellas and Jazz; Research Funding from RACE oncology and Otsuka/Astex. N.A.B. receives research funding from Merck KGaA and Bristol Myers Squibb.

Abstract

DNA hypomethylating agents (HMAs) are used to treat acute myeloid leukemia (AML) and myelodysplasia patients who are unsuitable for intensive chemotherapy. However, low response rates and therapy-resistant relapse remain significant challenges. To improve outcomes, we must understand how AML cells survive HMA treatment and continue to proliferate following therapy. We combine single-cell multiomics with parallel colony-forming assays to link HMA-induced heterogeneity with functional consequences in AML cellss. Azacytidine (AZA) and decitabine (DAC) induced global epigenetic heterogeneity, associated with upregulation of inflammatory responses and cell death pathways in a subset of hypomethylated cells. Some cells maintained high DNA methylation levels during treatment, and these methylation-retaining cells had increased self-renewal capacity following DAC treatment in two *FLT3-ITD* AML cell lines. Transcriptional profiling of colonies formed after HMA treatment revealed many genes with altered expression in both methylation-retaining and hypomethylated cells, with increased expression of cholesterol-related genes observed in all cell lines. Inhibition of the cholesterol biosynthesis pathway by rosuvastatin enhanced HMA effects on colony formation *in vitro* and extended survival in two *in vivo* models of AML. Our study demonstrates that HMA-induced epigenetic heterogeneity has implications for AML cell growth and identifies statins as a candidate co-treatment strategy to improve HMA efficacy.

Introduction

Hypomethylating agents (HMAs), such as azacytidine (AZA, 5-azacytidine) and decitabine (DAC, 2'-deoxy-5-azacytidine), are used to treat patients with acute myeloid leukemia (AML) and myelodysplastic syndrome (MDS) (1). AZA and DAC are cytidine analogs, which are incorporated into DNA during replication (1, 2). This leads to the degradation of DNA methyltransferase (DNMT) enzymes (3) and loss of DNA methylation in subsequent cell divisions (2, 4). HMA mechanisms of

action have been difficult to precisely define because genome-wide loss of methylation is associated with pleiotropic transcriptional changes (5). HMA-induced promoter hypomethylation permits the re-expression of tumor suppressor genes (6), re-activation of DNA repair pathways (7) and upregulation of differentiation markers in AML cells (8). HMA treatment can also increase the expression of cancer testis antigens (9) and enhance antigen presentation in cancer cells (10). Furthermore, genome-wide de-repression of transposable elements (TEs) has been shown to trigger a viral mimicry response, in which dsRNA stimulates interferon signaling and apoptosis (11-13). Unlike DAC, AZA can also be incorporated into RNA, which influences transcript stability and translation (14, 15).

While single-agent HMA treatment extends survival in many patients (16-18), only 20% show a complete response (CR) to therapy (19). Responses are also short-lived (e.g., 8-15 months (20)), with most patients developing HMA-resistant relapse. To address these limitations, clinical trials have tested co-treatment strategies, with some delivering improved outcomes (5). For example, the pro-apoptotic therapy venetoclax has increased response rates in elderly AML patients undergoing HMA treatment (21). However, relapse remains a significant problem, with the median duration of response being 11-18 months for patients treated with both venetoclax and HMA therapy (21, 22). To improve the long-term benefits of HMA therapy, it is essential to understand how AML cells survive treatment and proliferate to cause relapse.

In this study, we characterize HMA-induced molecular heterogeneity with implications for the self-renewal capacity of AML cells. We perform single-cell multiomic analysis to reveal global HMA-induced DNA methylation heterogeneity and methylation-retaining cells that appear to evade treatment. In parallel colony-forming assays, we show that methylation-retaining cells have a growth and self-renewal advantage following treatment with DAC, but not AZA, in two *FLT3-ITD* cell lines. We also identify the upregulation of cholesterol-related genes in colonies formed after HMA

treatment, and identify statins as a candidate treatment strategy to enhance the long-term efficacy of HMAs.

Results

DNA methylation heterogeneity induced by HMA treatment

We performed single-cell analysis of DNA methylation in AML cell lines (HL-60, MOLM-13, and MV-4-11; Supplementary Table 1) treated with low doses of decitabine (DAC) or azacytidine (AZA) to induce maximal demethylation with minimal effects on cell growth and viability (Supplementary Fig. S1). After three days of HMA treatment, a striking level of DNA methylation heterogeneity was observed (Fig. 1A; Supplementary Table 2). While untreated cells showed homogeneously high levels of DNA methylation (e.g., HL-60: 65-73%), the extent of hypomethylation varied substantially among cells treated with DAC (e.g., HL-60: 17-69%) or AZA (e.g., HL-60: 20-69%). Interestingly, a small proportion (1-5%) of methylation-retaining cells (Fig. 1A, dashed boxes) displayed no evidence of HMA-induced hypomethylation. The extent of HMA-induced hypomethylation was related to cell division rate, as indicated by positive correlations between DNA methylation and CellTrace fluorescence (Fig. 1B; Supplementary Fig. S2). This is consistent with HMA incorporation during replication (2) and confirms that slowly dividing cells can avoid the effects of HMA treatment.

Genomic contexts with high levels of DNA methylation in untreated HL-60 cells (such as exons, introns, and intergenic regions) showed the most pronounced reduction following HMA treatment (Fig. 1C), with this loss of methylation accompanied by increased cell-to-cell heterogeneity (Fig. 1D). In contrast, active promoters marked by H3K4me3 were the only genomic features to show a significantly decreased DNA methylation heterogeneity after HMA treatment, likely due to their low levels of DNA methylation in untreated cells.

To explore links between DNA methylation heterogeneity and other layers of genetic regulation, we used multi-omic data collected from HL-60 cells. The scNMT-seq method profiles DNA methylation, DNA accessibility, and gene expression in parallel (23), allowing these molecular modalities to be

correlated with each other across the genome of individual cells (Fig. 1E). Untreated cells showed the expected trends, with DNA methylation being negatively correlated with accessibility and gene expression, whereas DNA accessibility and transcription were positively correlated. In HMA-treated cells, the relationship between DNA methylation and accessibility was significantly weakened in all genomic contexts. HMA treatment also significantly weakened the correlation between DNA methylation (in promoters, exons, and introns) and expression of associated genes. In contrast, HMA treatment had a minimal effect on the association between DNA accessibility and gene expression. These observations imply that loss of DNA methylation is not always accompanied by increased accessibility and transcription.

Transcriptional programs linked to HMA-induced epigenetic heterogeneity

To clarify how HMA-induced epigenetic heterogeneity influences transcriptional responses, we performed a multivariate analysis to integrate the three molecular layers: DNA methylation, DNA accessibility, and transcription. We excluded untreated cells to focus on variability among HMA-treated cells and applied an unsupervised sparse Partial Least Squares (sPLS) method (27). This approach was used to identify variably expressed transcripts that are highly correlated to changes in DNA methylation and accessibility in regulatory regions (CpG islands, promoters, H3K4me3 sites, and H3K27ac sites) and 3kb genomic windows.

The 200 transcript features selected by sPLS were further examined in both treated and untreated cells, revealing 4 groups of cells with distinct transcriptional profiles (Fig. 2A, B). A significant and negative correlation (r = -0.37, $p < 1 \times 10^{-7}$) between TE LINE:L2a expression and component 1 was observed (Fig. 2C; Supplementary Fig. S3A), consistent with activation of viral mimicry in cell group 3. However, there was no significant relationship between global DNA methylation and component 1, and cell group 3 had similar methylation levels to other HMA-treated cells (Fig. 2D; Supplementary Fig. S3D). This indicates that global methylation levels are insufficient to explain the transcriptional responses of HMA-treated AML cells.

124 Gene ontology (GO) over-representation analysis (ORA) was performed for each of the three clusters
125 of transcript features (Fig. 2B; Supplementary Table 3). Cell group 3 had low expression of genes in
126 cluster 3, which were related to translation and inhibition of cell death (Fig. 2E; Supplementary Table
127 4). Cell group 3 also had high expression of genes in cluster 1, which were enriched in terms related
128 to immune inflammatory response and positive regulation of cell death (Fig. 2F; Supplementary
129 Table 4). This transcriptional profile is consistent with the expected effects of HMA treatment (1),
130 and 29 of the 78 genes in cluster 1 were significantly upregulated by DAC and/or AZA in matched
131 bulk RNA sequencing (RNA-seq) data (Supplementary Table 3). In contrast, cell group 1 displayed an
132 inverted gene expression pattern and included many untreated cells (observed:expected ratio =
133 1.48). This suggests that cell group 1 did not activate transcriptional pathways commonly associated
134 with HMA treatment, despite low methylation levels in most cells (Fig. 2A, D). The expression profile
135 of cell group 2 was intermediate between groups 1 and 3, whereas cell group 4 showed distinctive
136 upregulation of genes expressed in cluster 2. No ontology terms from cluster 2 retained significance
137 after multiple testing correction.

138 The sPLS model also selected epigenetic features that were correlated to the 200 transcript features,
139 without considering the direction of correlation nor the proximity of features (Tables S5, S6). For cell
140 group 3, the selected DNA methylation features have low methylation in many cells, whereas the
141 DNA accessibility features tend to have high accessibility (Fig. 2B, G). This was in contrast to other
142 cell groups, suggesting that the transcriptional response to HMA treatment is associated with
143 reductions in DNA methylation and gains in accessibility. Consistently, transcript features from
144 expression cluster 1 had predominantly positive correlations with accessibility features and many
145 negative correlations with methylation features, especially in CpG islands and 3kb genomic windows
146 (Supplementary Fig. S4).

147 To test whether epigenetic alterations in *cis*-regulatory elements could influence transcriptional
148 responses to HMA treatment, we next correlated gene expression with DNA methylation and

accessibility in nearby genomic loci. Genes from expression cluster 1 showed a significant shift toward negative correlations with promoter methylation ($p = 2.15 \times 10^{-11}$, χ^2 test) and positive correlations with promoter accessibility ($p = 2.26 \times 10^{-8}$, χ^2 test), suggesting that these genes are particularly sensitive to loss of DNA methylation in *cis* (Fig. 2H, I; Supplementary Table 7). An interesting example is *RHEX* (regulator of hemoglobinization and erythroid cell expansion), which is highly expressed in AML (32). Negative correlations between *RHEX* expression and DNA methylation were concentrated in a promoter-proximal region of intron 1, which contains several conserved long terminal repeat (LTR) TEs (Fig. 2I).

In summary, our single-cell multiomic analysis identified transcriptional changes linked to patterns of epigenetic heterogeneity in HMA-treated AML cells. Importantly, activation of genes involved in inflammatory response and cell death pathways (expression cluster 1) was observed in only a subset of hypomethylated cells (cell group 3) (Fig. 2A, C, D).

Effects of HMA-induced heterogeneity on the self-renewal capacity of AML cells

To determine the consequences of epigenetic and transcriptional heterogeneity on AML cell self-renewal, colony-forming assays were performed. DAC and AZA significantly decreased colony counts (Fig. 3A), as previously reported (33). DAC treatment also significantly increased the size of colonies in the two *FLT3-ITD* cell lines, MOLM-13 and MV-4-11 (Supplementary Table 1, Fig. S5A). To characterize the molecular profiles of colonies formed after HMA treatment, we performed single-colony analysis of DNA methylation (Fig. 3B-C; Supplementary Table 8). Following DAC treatment (Fig. 3B, solid fill) many colonies (34-65%) had DNA methylation levels comparable to untreated colonies (≥75%). This was in stark contrast to the low percentage of methylation-retaining cells (1-5%) observed in single-cell data after 72h of DAC treatment (Fig. 1A, dashed box; Fig. 3B, dashed line). Surprisingly, this shift toward higher DNA methylation levels was far less pronounced in colonies established following AZA treatment (Fig. 3C).

To assess the recovery of DNA methylation following HMA treatment, time-course analysis was performed during colony formation (Fig. 3D). DNA methylation levels in HMA-treated HL-60 colonies were low throughout the time course (Fig. 3D, top), mirroring an analysis performed in suspension culture (Supplementary Fig. S1E). Similar results were obtained for MOLM-13 and MV-4-11 colonies derived after AZA treatment (Fig. 3D, center and bottom). In contrast, high levels of DNA methylation were observed in the early stages of colony formation (experiment day 6) following DAC treatment of MOLM-13 and MV-4-11 cells (Fig. 3D, center and bottom). This suggests that the shift toward high DNA methylation observed in these colonies (Fig. 3B) was not due to gradual recovery of methylation. Rather, our data are consistent with the selection of highly methylated cells in colony-forming assays performed after DAC treatment. We deduce that methylation-retaining cells can have increased self-renewal and proliferative capacity relative to hypomethylated cells after HMA treatment, but this may depend on the mutational profile of the AML cells and the HMA used.

Transcriptional changes in hypomethylated and methylation-retaining colonies

Next, we generated matched transcriptomes from the same set of colony samples (Supplementary Table 8). Single-colony RNA-seq and principal component analysis (PCA) showed that DAC and AZA samples were generally distinct from untreated samples, regardless of their global DNA methylation levels, in all cell lines (Fig. 4A). This implies that HMA exposure has substantial effects on the transcriptome, even in highly methylated cells.

Of the 2000 most variably expressed genes among the HL-60 samples, only 215 had increased expression specific to hypomethylated colonies (Fig. 4B, cluster 3; Supplementary Table 9). Many of these genes (42.3%) were upregulated after 72h of treatment with either DAC or AZA in bulk HL-60 RNA-seq data, and several were associated with activation of inflammatory responses within the sPLS model (e.g., *S100A8* and *S100A9*; Supplementary Table 9; Fig. 2B, cluster 1). In contrast, the genes in cluster 5 were upregulated following HMA exposure in both hypomethylated and highly methylated colonies (Fig. 4B), and only 3.5% of these genes were induced by HMA treatment in bulk

RNA-seq data (Supplementary Table 9). Thus, some transcriptional changes that occur immediately after HMA treatment are maintained in hypomethylated colonies, whereas other genes are upregulated during colony formation and are independent of HMA-induced global hypomethylation. GO ORA revealed an enrichment of anti-microbial and immune-related processes among both hypomethylation-dependent and -independent gene sets, whereas 'small molecule biosynthetic process' and 'cholesterol biosynthetic process' were over-represented among the hypomethylation-independent cluster 5 genes (Fig. 4C; Supplementary Table 10). HL-60 colonies that retained DNA methylation following DAC treatment also had particularly high expression of cholesterol-related genes, including many enzymes required for *de novo* cholesterol biosynthesis downstream of mevalonate (34) (Supplementary Fig. S6-7; Tables S11, S12).

We next performed a focused analysis of genes annotated to 'cholesterol biosynthetic process' (GO:0006695) across all cell lines. Like HL-60 colonies, MOLM-13 and MV-4-11 samples displayed increased expression of many of these genes after HMA treatment (Supplementary Fig. S8). Furthermore, a statistical analysis revealed that 5 genes (*SREBF1*, *SCAP*, *PMVK*, *MVD* and *LSS*) were significantly increased (Pairwise Wilcoxon test with Benjamini-Hochberg correction, FDR = < 0.05) by both DAC and AZA in colonies derived from all 3 cell lines (Fig. 5A). These genes form part of a regulatory feedback loop that maintains cholesterol homeostasis by up-regulating biosynthesis in response to low cellular cholesterol (35) (Supplementary Fig. S6). Since cholesterol regulation is altered in both methylation-retaining and hypomethylated colonies, targeting this metabolic pathway could overcome the initial heterogeneity induced by HMA treatment (Fig. 1-3).

Inhibition of cholesterol pathways following HMA exposure

To further investigate the relationship between cholesterol regulation and self-renewal capacity following HMA treatment, we performed colony-forming assays in the presence of rosuvastatin. Rosuvastatin is a potent inhibitor of the rate-limiting enzyme of the cholesterol biosynthetic pathway, HMG-CoA reductase (HMGCR), and is frequently prescribed to reduce the risk of

224 cardiovascular diseases associated with hypercholesterolaemia (36). AZA and rosuvastatin co-
225 treatment had varied effects in AML cell lines (Fig. 5B, C), with synergistic effects on colony-
226 formation observed in MV-4-11 cells (Supplementary Fig. S5C). Meanwhile, DAC and rosuvastatin
227 had synergistic effects on colony formation in all cell lines (Supplementary Fig. S5C), with
228 significantly fewer colonies formed upon addition of 10 or 30 µM rosuvastatin in MOLM-13 cells (Fig.
229 5B). Colonies also displayed significantly reduced size (Supplementary Fig. S5B) and DNA methylation
230 levels (Fig. 5C) following DAC and rosuvastatin treatment of MOLM-13 and MV-4-11 cell lines, where
231 strong selection for highly methylated cells was previously noted (Fig. 3B). This suggests that
232 inhibition of cholesterol biosynthesis is effective even against methylation-retaining cells that
233 maintain self-renewal capacity following HMA treatment.

234 The efficacy and potential clinical utility of DAC and rosuvastatin co-treatment was then tested in
235 immunocompromised mice engrafted with luciferase-tagged MOLM-13 cells. In a dose optimization
236 experiment, combining DAC and rosuvastatin led to a significant increase in median survival for all
237 doses tested (Fig. 6A; Supplementary Table 13). The 1 mg/kg/day dose of rosuvastatin was chosen
238 for further validation in this model, as it is a low dose commonly prescribed for preventing
239 cardiovascular disease (equivalent to approximately 5mg/day oral dose in humans). Co-treatment
240 with DAC and rosuvastatin once again led to a significant increase in median survival compared to
241 DAC treatment alone (24 vs. 21 days) in this aggressive *in vivo* AML model (Fig. 6B; Supplementary
242 Table 14). In contrast, rosuvastatin alone significantly reduced the median survival time of vehicle-
243 treated mice (18 vs. 19 days; Fig. 6B; Supplementary Table 14). Finally, we assessed AZA and DAC in
244 combination with rosuvastatin in a patient-derived xenograft model of AML (AML-16). Rosuvastatin
245 (1mg/kg/day) co-treatment significantly extended the median survival of AZA-treated mice by 8.5
246 days (Fig. 6C; Supplementary Table 15) and decreased leukemia burden (Fig. 6D). Meanwhile,
247 combining rosuvastatin with DAC (0.2mg/kg/day) had no significant effect on survival or leukemia
248 burden in this model (Supplementary Fig. S9). These *in vivo* results provide evidence that HMAs

249 combined with statins have the potential to decrease leukemia burden and improve AML survival,
250 with further research required to optimize drug selection and dosing in patient cohorts.

251 Discussion

252 A thorough understanding of the ways in which AML cells survive HMA therapy and initiate
253 recurrence is essential to overcome the clinical challenge of treatment-resistant relapse. Our unique
254 study has revealed HMA-induced heterogeneity and methylation-retaining cells that evade the
255 epigenetic effects of treatment. We also identify metabolic pathways associated with the self-
256 renewal of HMA-treated AML cells, which can be targeted to improve HMA effects.

257 Our single-cell multiomic analyses revealed global DNA methylation heterogeneity induced by
258 treatment and transcriptional responses linked to epigenetic changes. We observed activation of
259 inflammatory response and cell death pathways in only a minor subset of hypomethylated cells (Fig.
260 2B), consistent with our previous report of heterogeneous TE expression following DAC treatment
261 (24) and scRNA-seq data from a colorectal cancer cell line (37). These observations suggest that
262 additional epigenetic modifications, transcription factors, or other mechanisms can suppress
263 transcriptional responses in hypomethylated cells (e.g., H3K9me3 (38, 39)). Alternatively, loss of
264 methylation at specific loci may be required for HMAs to exert their effects. Our observations are
265 consistent with the lack of correlation between HMA-induced global hypomethylation and clinical
266 response (40, 41) and support the use of locus-specific methylation changes to build a predictor of
267 patient response (42).

268 In contrast to our single-cell analyses, Li *et al.* reported reduced epigenetic and transcriptional
269 variance in AML cells collected after 12 weeks of AZA treatment in a transgenic mouse model (43).
270 We suggest that HMAs initially increase epigenetic and transcriptional diversity, allowing some cells
271 to gain a relative growth or survival advantage. Subsequent expansion of these clones would lead to
272 reduced heterogeneity, as reported by Li *et al.* (43). Consistently, we found that some AML cells
273 retained high levels of DNA methylation during HMA treatment (Fig. 1A) and had a relative growth

274 advantage following drug withdrawal (Fig. 3). Methylation-retaining cells tended to divide less
275 frequently during treatment (Fig. 1B) but had higher self-renewal and proliferative capacity than
276 hypomethylated cells after DAC treatment (Fig. 3). Interestingly, this selection for methylation-
277 retaining cells was less pronounced following AZA treatment, reflecting previous reports of distinct
278 effects of these HMAs (44, 45). Since AZA is incorporated into both DNA and RNA (46), whereas DAC
279 is restricted to DNA, we speculate that RNA-mediated toxicities (such as translational inhibition (14,
280 15)) could prevent the growth of highly methylated cells following AZA treatment. Taken together,
281 our results show that heterogeneous responses to HMA treatment can influence AML cell self-
282 renewal with potential implications for relapse.

283 We observed upregulated expression of cholesterol biosynthesis genes in colonies formed after
284 HMA treatment (Fig. 5; Supplementary Fig. S6, 8). These changes were observed in both
285 hypomethylated and highly methylated colonies, suggesting that HMA exposure has persistent
286 transcriptional effects that are independent of global methylation loss. Rapidly proliferating AML
287 cells are known to have high cholesterol demands (47), with cholesterol and related metabolites
288 required for cell membrane synthesis, lipid rafts, cell cycle progression and activation of oncogenic
289 signaling molecules (via prenylation of RAS, Rho/Rac) (Supplementary Fig. S7) (34, 48). In colony-
290 forming assays rosuvastatin synergistically enhanced the effects of DAC (Fig. 5B; Supplementary Fig.
291 S5C), suggesting that rapid consumption of cholesterol supports AML cell self-renewal after HMA
292 treatment (35). Since this metabolic adaptation occurs even in highly methylated cells, statin co-
293 treatment could have broad impact to inhibit AML cell growth despite initial heterogeneity in HMA
294 responses.

295 Altered cholesterol regulation is an established feature of AML with relevance to prognosis and
296 therapy (47, 49, 50). Recently, cholesterol metabolism was also linked to DAC resistance in AML cell
297 lines, with statin co-treatment showing synergistic inhibition of *in vitro* AML cell growth (51). Others
298 have shown that inhibition of cholesterol biosynthesis can sensitize AML cells to radiation and

chemotherapy (52, 53). *In vivo*, we observed significantly improved survival of leukemia-bearing mice treated with HMA and rosuvastatin (Fig. 6) suggesting that co-treatment may increase the duration of response in some AML and MDS patients. Encouragingly, a recent retrospective analysis of MDS patients (including some HMA-treated high-risk cases) reported improved survival and reduced progression to AML in patients who commenced statin treatments three months before or after MDS diagnosis (54). Current clinical trials are testing the safety of a statin (pitavastatin) in combination with AZA and venetoclax in AML patients (55). This therapeutic avenue is of particular interest since statins are commonly prescribed, well-tolerated, oral medications, which could be rapidly repositioned for use in AML and MDS patients receiving HMA therapy. Our results support further investigation of the long-term benefits of statin and HMA co-treatments in different AML subtypes.

Methods

Cell lines and culture

AML cell lines (Supplementary Table 1), HL-60 (ATCC #CCL-240), MOLM-13 (DSMZ #ACC-554), and MV-4-11 (ATCC #CRL-9591), were maintained in tissue culture flasks (Greiner Bio-One) at 37°C and 5% CO_2, and sub-cultured at 500,000 cells/mL every 2-3 days with fresh medium. HL-60 cells were maintained in Iscove's Modified Dulbecco's medium (IMDM; Sigma-Aldrich) supplemented with 4mM GlutaMAX (Thermo Fisher Scientific) and 10% Fetal Bovine Serum (FBS; Sigma-Aldrich). MOLM-13 and MV-4-11 cells were maintained in Roswell Park Memorial Institute 1640 medium (RPMI; Sigma-Aldrich) supplemented with 2mM GlutaMAX and 10% FBS.

CellTrace staining

AML cells (2-2.5x10^6 cells/mL) were stained with 1µM (MOLM-13 and MV-4-11) or 3µM (HL-60) CellTrace Far Red (Thermo Fisher Scientific), according to the manufacturer's instructions. MOLM-13 and MV-4-11 cells with uniformly high CellTrace fluorescence were purified by fluorescence-

activated cell sorting (FACS) prior to treatment with hypomethylating agents (HMAs), whereas all cells were used for HL-60 treatments.

HMA treatments

HMA treatments were performed in suspension culture, with drugs added every 24h for 72h total. All cell lines were treated with 100nM decitabine (DAC; Selleckchem #S1200), HL-60 cells were treated with 2000nM azacytidine (AZA; Selleckchem # S1782), while MOLM-13 and MV-4-11 cells were treated with 500nM AZA. Untreated cells (UNT) received 0.1% DMSO (vehicle control).

Fluorescence activated cell sorting (FACS)

HMA-treated cells were stained with propidium iodide (PI, 1.5µg/mL) and prepared for FACS. Viable (PI^-) single cells were sorted into 2.5µL of RLT PLUS buffer (Qiagen) containing 2.5U SUPERas-In (Thermo Fisher Scientific) in 96-well plates using indexed sorting on a FACS Aria II (BD Biosciences). Plates were sealed and briefly centrifuged before storage at -80°C for sequencing analysis.

Colony-forming assays

HMA-treated cells were seeded in MethoCult Optimum (H4034; STEMCELL Technologies Inc.) at 500 cells/well in 6-well plates with rosuvastatin (Selleckchem # S2169) added to the MethoCult at various doses (0, 1, 10, 30µM). Cells were cultured at 37°C and 5% CO_2 for 14 days, and colonies were imaged using Cytation3 (Biotek). Colony counts and sizes were analyzed using ImageJ software. Individual colonies were manually plucked using a 20µL pipette tip into 100µL of media, centrifuged at 200xg for 5 min, and then resuspended in 20µL of RLT PLUS buffer before storage at -80°C. Alternatively, all colonies in each well were collected by resuspending the MethoCult Optimum media (and colonies) in 3mL of standard culture media (IMDM or RPMI), centrifuging at 200xg for 5 min, and resuspending the cell pellet in 20-50µL of RLT PLUS buffer before storage at -80°C.

Library preparation and sequencing

scNMT-seq library preparation and sequencing

For scNMT-seq, matched scNOMe-seq and scRNA-seq libraries were prepared from sorted HL-60 single cells as previously described (23). Minor modifications to the published protocol were as follows: 1) Amplified cDNA was purified using a 0.6:1 volumetric ratio of AMPure XP Beads (Beckman Coulter) and eluted in 15µL water. 2) During the fifth repeat of first-strand synthesis reaction, the samples were held at 37°C for 90min. 3) The oligo used in the second-strand synthesis reaction (5'-CAGACGTGTGCTCTTCCGATCTNNNNNN-3') was modified to be compatible with the NEBNext oligos (multiplex oligos for Illumina, dual index sets, New England Biolabs), which were used to amplify scNOMe-seq libraries. 4) A 0.65:1 volumetric ratio of AMPure XP Beads was used to purify products of both the first- and second-strand synthesis reactions, as well as the amplified scNOMe-seq libraries.

For scNOMe-seq libraries, paired-end 150bp sequencing was performed using the NovaSeq (Illumina) platform. For scRNA-seq libraries, paired-end 75bp sequencing was performed on the NovaSeq or NextSeq (Illumina) platform.

scTEM-seq library preparation and sequencing

For scTEM-seq analysis of global DNA methylation levels in single MOLM-13 and MV-4-11 cells, library preparation was performed as described (24). Paired-end 150bp sequencing was performed on the MiSeq (Illumina) platform.

Colony TEM-seq and RNA-seq library preparation and sequencing

Single-colony TEM-seq (Fig. 3B, C) and parallel RNA-seq analyses were performed as described (24, 25) with minor modifications. Lysates from single colonies (HL-60: 7.5µL; MOLM-13 and MV-4-11: 2.5µL) were used to separate genomic DNA and mRNA. During single-colony TEM-seq library preparation, the number of SINE Alu amplification cycles was reduced to 29. For RNA-seq analysis, 15 cycles of cDNA amplification were performed.

TEM-seq analysis of pooled colonies (Fig. 3D, 5E) was performed as described (25) using 5-10µL of cell lysate as input for bisulfite conversion and 29 cycles for SINE Alu amplification.

TEM-seq libraries were sequenced using 150bp paired-end sequencing on the MiSeq platform. For RNA-seq libraries, paired-end 75bp sequencing was performed on the NextSeq or NovaSeq platform.

Data processing

Sequencing data were processed and aligned as described in the Supplementary Information.

scNMT-seq data analysis

Quality control, data normalization and batch correction were performed as described in the Supplementary Information. All analyses were performed in R v4.2.1, unless otherwise stated.

Pairwise distance analysis of DNA methylation heterogeneity

To assess DNA methylation heterogeneity per treatment group and genomic context (Fig. 1D), pairwise CpG methylation distance analysis was performed. The mean absolute methylation difference was computed for each cell pair (A, B) as the mean of the absolute difference in methylation rate at each common cytosine position in the relevant genomic annotation. To make the comparison of methylation patterns meaningful, only cytosine loci with data from both cells in the pair were used. The mean absolute methylation differences were grouped according to the treatment combination of the cell pairs. The global summaries shown in Fig. 1D correspond to groups in which both cells in the pair had the same treatment. Higher values indicate a more heterogeneous methylation pattern when cells in the same treatment group were compared vis-à-vis.

Cell-wise correlation analysis

To assess the relationships between DNA methylation, DNA accessibility, and gene expression within individual cells (Fig. 1E), Pearson correlations were computed using HL-60 scNMT-seq data. For this analysis, RNA-seq data was normalized and log transformed per batch using ‘scuttle::logNormCounts()’ (v1.6.2) (26) without batch correction or prior count filtering. DNA

395 methylation was correlated to DNA accessibility at matched loci, based on genomic co-ordinates. For
396 correlations with gene expression, methylation and accessibility measurements at promoters,
397 introns, and exons were matched to the corresponding transcript. For CpG islands, H3K27ac sites
398 and H3K4me3 sites, methylation and accessibility measurements were matched to all transcripts
399 within 10kb. For intergenic regions and 3kb genomic windows, methylation and accessibility
400 measurements were matched to every transcript within 1bp to assess the expression of immediately
401 adjacent genes. For each cell, Pearson's correlation estimates were then computed using all
402 matched values and the 'cor.test()' function in R.

403 **Integrative sparse partial least squares (sPLS) analysis**

404 Mixomics (27) (v6.20.0) was used to perform a multivariate integrative analysis of the HL-60 scNMT-
405 seq data (Fig. 2A-D). Feature selection was performed to identify variably expressed transcripts that
406 were highly correlated with changes in DNA Methylation and accessibility after HMA treatment. We
407 performed an unsupervised sparse Partial Least Squares (sPLS) analysis using the function
408 'mixOmics::mint.block.spls()' which combines a multivariate integrative (MINT) method and a
409 multiblock sPLS integrative analysis. MINT (28) accounts for multiple batches (Supplementary Table
410 2) measured on the same variables, while the multiblock sPLS seeks for correlated patterns between
411 DNA methylation and DNA accessibility rates that are split into multiple genomic regions ('blocks')
412 and explain (correlated to) the predictor (transcriptome).

413 To focus on transcriptomic and epigenetic changes resulting from HMA treatment, only treated cells
414 (AZA and DAC) were included in the sPLS model. The genomic regions included in this analysis for
415 both DNA methylation and DNA accessibility were CpG islands, promoters, H3K27ac sites, H3K4me3
416 sites and 3kb windows. The rates from these genomic regions were filtered to retain only those
417 detected in greater than 10% of cells. The sPLS model was implemented assessing two components,
418 selecting 50 features per component and per block (genomic region) in the DNA methylation and

419 DNA accessibility datasets, and 100 genes per component in the transcriptome dataset. Further
420 details are provided on GitHub.

421 Heatmap visualization and identification of cell and expression clusters from sPLS-selected features
422 was performed using the ComplexHeatmap package (v2.12.1). sPLS selected features for
423 components 1 and 2 were extracted using the function 'mixOmics::selectVar()'. Heatmap
424 visualization was performed on sPLS-selected features using transcriptomic (converted to z-score)
425 and epigenetic rates (mean of features in genomic regions and converted to z-score) that were
426 entered into the model and included both treated and untreated cells. K-means clustering was
427 performed on sPLS-selected transcriptomic features, first on Gene Expression (row_km=3), followed
428 by Cell Group (column_km=4).

429 sPLS sample projections (Fig. 2A, C, and D) were plotted using ggplot2 (29) (v3.3.6) by extracting the
430 sPLS components 1 and 2 for a given block (RNA or epigenetic genomic region) and overlaid with
431 relevant information, that is, the cell group identified from k-means clustering and treated cell type
432 or average DNA methylation.

433 Gene Ontology (GO) Over Representation Analysis (ORA) was calculated using clusterProfiler (30)
434 (v4.4.4) for 'biological process' and displayed using enrichplot (v1.16.1) (Fig. 2E, F). Gene Expression
435 k-means clusters (Fig. 2B) and sPLS selected features per component (1-2) were assessed by
436 'enrichGO(p.adj=0.05, p.adj.method = "fdr", q.val.threshold = 0.4)' and the list of genes from the
437 batch corrected transcriptome dataset (entered into the sPLS model) as the background. Results
438 were displayed as treeplots using default settings for pairwise 'termsim()' and 'treeplot(nCluster=5,
439 showCategory = 10)'.

440 The correlation of sPLS features (Supplementary Fig. S3) was calculated as a similarity matrix using
441 'mixOmics::circosPlot()' on the sPLS model. The results were displayed using ComplexHeatmap,
442 showing DNA methylation and DNA accessibility features related to transcript features split by the
443 previously identified Gene Expression k-means clusters.

Locus-specific correlation analysis

To compare gene expression to adjacent epigenetic features, locus-specific correlations were performed using HL-60 scNMT-seq data (Fig. 2H, I). DNA methylation and DNA accessibility measurements were paired to genes based on annotation (promoters) or by strand-aware position within 10kbp of the gene transcription start site (CpG islands, H3K27ac sites, H3K4me3 sites and 3kb windows). For paired sites, Pearson's correlations were computed between CpG or GpC methylation rate and log gene expression values. All cells with data (i.e., the UNT, DAC, and AZA groups) were combined in these correlations, and a minimum of 22 cells with paired data (i.e., both gene expression and DNA methylation/accessibility measurements) were required for the correlation to be performed.

Colony sequencing analysis

Quality control, data normalization and batch correction were performed as described in the Supplementary Information. All analyses were performed in R v4.2.1.

Highly variable gene analysis

For Figure 4, highly variable genes (HVGs) were identified from colony RNA-seq data and principal component analysis (PCA) was performed using 'scater::calculatePCA(ntop = 2,000)'. K-means clusters of HVGs were determined using the R stats package (v4.2.1) with 'kmeans(centers = 8, iter.max = kmeans.iter, nstart = 50)'. Heatmapping of HVGs and k-means cluster was performed using 'ComplexHeatmap::pheatmap()' with z-scored values and Euclidean distance hierarchical clustering within row clusters (k-means groups) and columns (samples) ordered by treatment and descending average global methylation level.

GO ORA of k-means clusters was compared using clusterProfiler for 'biological process' by 'compareCluster(pAdjustMethod = "fdr", p.adj.threshold = 0.05, qvalueCutoff=0.4)' and the full list of genes from the batch corrected dataset (for each cell type) as the background list. Plots were created using 'clusterProfiler::dotplot(showCategory = 3) + coord_flip()'.

Analysis of cholesterol biosynthesis gene expression

For Figure 5A, genes from the cholesterol biosynthesis pathway (GO:0006695) were analyzed from batch corrected expression data for each cell line (HL-60, MOLM-13 and MV-4-11). After batch correction, 40 genes out of 58 genes (from GO:0006695) were in common across all three cell lines datasets. In total, for each cell line there were 41 (HL-60), 41 (MOLM-13) and 43 (MV-4-11) genes analyzed from GO:0006695. The R package rstatix (v0.7.2) was used to perform pairwise Wilcoxon test between treatment groups with UNT samples as the reference group for each gene. Benjamini-Hochberg false discovery rate (FDR) correction was performed on all p-values, per cell line. Boxplots were generated using ggpubr (v0.6.0) displaying the batch corrected relative expression with 'pointrange' error.

AML xenograft models

Five-week-old female NOD.Cg-Prkdc scid Il2rg tm1Wjl /SzJ (NSG) mice were obtained from the Australian Bioresources (ABR, Moss Vale, NSW, Australia) and acclimatized for one week prior to any experimental procedure.

MOLM-13 cells transduced with firefly luciferase (MOLM-13-luc; $5x10^5$ cells suspended in 100 µL of PBS) were injected into the lateral tail vein of NSG mice. Leukemia burden was assessed by bioluminescence imaging (BLI) twice a week using an IVIS Spectrum *in vivo* imaging system (PerkinElmer, Waltham, MA, USA), following intraperitoneal injections of 150 mg/kg D-luciferin (Promega, Alexandria, NSW, Australia) under anesthesia with isoflurane. Treatments commenced on day 6 post-engraftment when a positive luminescence signal was detected. Mice (*n* = 5-15/group) were treated by intraperitoneal injection of either vehicle (2% DMSO, 30% PEG300 in water), DAC (0.2 mg/Kg in saline), rosuvastatin (1 mg/kg), or combination rosuvastatin (1 mg/kg, 10 mg/kg, or 40 mg/kg in 30% PEG300 in water) and DAC (0.2 mg/Kg) once a day (5 days on, 2 days off) for up to 3 weeks. The animals were monitored until they reached the ethical endpoint.

For patient derived xenograft (PDX) experiments, NSG mice were inoculated with $2x10^6$ AML-16 cells (*FLT3-ITD*, *NPM1*, *IDH2*, and *WT1* mutant) (31) in 100µL of PBS, by injection into the lateral tail vein. Leukemia burden (% hCD45+ cells in peripheral blood) was assessed 1-2 times weekly via flow cytometry (FACSCanto II). Treatment commenced once an average leukemia burden of 1% $CD45^+$ cells was achieved (~3.5 weeks). Mice (n= 6-11 per group) received vehicle (2% DMSO, 30% PEG300 in water), DAC (0.2 mg/Kg), AZA (1mg/Kg), rosuvastatin (1 mg/kg), DAC + rosuvastatin, or AZA + rosuvastatin, via intraperitoneal injections once a day (5 days on, 2 days off) for 1 week (cycle 1), followed by twice per week for an additional 2 weeks (2 cycles). Mice were monitored until the ethical endpoint (>25% $huCD45^+$ cells).

Survival Analysis

Survival analyses were performed using Kaplan-Meier analysis followed by the log-rank (Mantel-Cox) test. All statistical analyses were performed using GraphPad Prism v. 9.0 (GraphPad Software, La Jolla, CA, USA). Differences were considered statistically significant at an adjusted p-value < 0.05.

Data Availability

Sequencing data generated in this study has been deposited in the GEO database (GSE255339). Relevant code for this manuscript is available on GitHub via:

www.github.com/canepi/HMA_heterogeneity

References

1. Stomper J, Rotondo JC, Greve G, Lübbert M. Hypomethylating agents (HMA) for the treatment of acute myeloid leukemia and myelodysplastic syndromes: mechanisms of resistance and novel HMA-based therapies. Leukemia. 2021.

2. Jones PA, Taylor SM. Cellular differentiation, cytidine analogs and DNA methylation. Cell. 1980;20(1):85-93.

516 3. Patel K, Dickson J, Din S, Macleod K, Jodrell D, Ramsahoye B. Targeting of 5-aza-2-
517 deoxycytidine residues by chromatin-associated DNMT1 induces proteasomal degradation of the
518 free enzyme. Nucleic Acids Research. 2010;38(13):4313-24.
519 4. Issa JP, Roboz G, Rizzieri D, Jabbour E, Stock W, O'Connell C, et al. Safety and tolerability of
520 guadecitabine (SGI-110) in patients with myelodysplastic syndrome and acute myeloid leukaemia: a
521 multicentre, randomised, dose-escalation phase 1 study. Lancet Oncol. 2015;16(9):1099-110.
522 5. Fennell KA, Bell CC, Dawson MA. Epigenetic therapies in acute myeloid leukemia: where to
523 from here? Blood. 2019;134(22):1891-901.
524 6. Daskalakis M, Nguyen TT, Nguyen C, Guldberg P, Kohler G, Wijermans P, et al.
525 Demethylation of a hypermethylated P15/INK4B gene in patients with myelodysplastic syndrome by
526 5-Aza-2'-deoxycytidine (decitabine) treatment. Blood. 2002;100(8):2957-64.
527 7. Kiziltepe T, Hideshima T, Catley L, Raje N, Yasui H, Shiraishi N, et al. 5-Azacytidine, a DNA
528 methyltransferase inhibitor, induces ATR-mediated DNA double-strand break responses, apoptosis,
529 and synergistic cytotoxicity with doxorubicin and bortezomib against multiple myeloma cells.
530 Molecular Cancer Therapeutics. 2007;6(6):1718-27.
531 8. Dunshee DR, Dai Y, Jang JC, Risueño A, Jeyaraju DV, Hagner P, et al. CC-486 Mechanism
532 Imparted By Extended Exposure of Azacitidine Upregulates Myeloid Differentiation Markers and
533 Induces Cell Death in AML Cells. Blood. 2020;136:33-4.
534 9. Goodyear O, Agathanggelou A, Novitzky-Basso I, Siddique S, McSkeane T, Ryan G, et al.
535 Induction of a CD8+ T-cell response to the MAGE cancer testis antigen by combined treatment with
536 azacitidine and sodium valproate in patients with acute myeloid leukemia and myelodysplasia.
537 Blood. 2010;116(11):1908-18.
538 10. Nahas MR, Stroopinsky D, Rosenblatt J, Cole L, Pyzer AR, Anastasiadou E, et al.
539 Hypomethylating agent alters the immune microenvironment in acute myeloid leukaemia (AML) and
540 enhances the immunogenicity of a dendritic cell/AML vaccine. Br J Haematol. 2019;185(4):679-90.

541 11. Roulois D, Loo Yau H, Singhania R, Wang Y, Danesh A, Shen SY, et al. DNA-Demethylating
542 Agents Target Colorectal Cancer Cells by Inducing Viral Mimicry by Endogenous Transcripts. Cell.
543 2015;162(5):961-73.
544 12. Liu M, Ohtani H, Zhou W, Orskov AD, Charlet J, Zhang YW, et al. Vitamin C increases viral
545 mimicry induced by 5-aza-2'-deoxycytidine. Proc Natl Acad Sci U S A. 2016;113(37):10238-44.
546 13. Chiappinelli Katherine B, Strissel Pamela L, Desrichard A, Li H, Henke C, Akman B, et al.
547 Inhibiting DNA Methylation Causes an Interferon Response in Cancer via dsRNA Including
548 Endogenous Retroviruses. Cell. 2015;162(5):974-86.
549 14. Aimiuwu J, Wang H, Chen P, Xie Z, Wang J, Liu S, et al. RNA-dependent inhibition of
550 ribonucleotide reductase is a major pathway for 5-azacytidine activity in acute myeloid leukemia.
551 Blood. 2012;119(22):5229-38.
552 15. Diesch J, Le Pannérer M-M, Winkler R, Casquero R, Muhar M, van der Garde M, et al.
553 Inhibition of CBP synergizes with the RNA-dependent mechanisms of Azacitidine by limiting protein
554 synthesis. Nature Communications. 2021;12(1):6060.
555 16. Fenaux P, Mufti GJ, Hellstrom-Lindberg E, Santini V, Finelli C, Giagounidis A, et al. Efficacy of
556 azacitidine compared with that of conventional care regimens in the treatment of higher-risk
557 myelodysplastic syndromes: a randomised, open-label, phase III study. Lancet Oncol.
558 2009;10(3):223-32.
559 17. Fenaux P, Mufti GJ, Hellström-Lindberg E, Santini V, Gattermann N, Germing U, et al.
560 Azacitidine prolongs overall survival compared with conventional care regimens in elderly patients
561 with low bone marrow blast count acute myeloid leukemia. J Clin Oncol. 2010;28(4):562-9.
562 18. Kantarjian HM, O'Brien S, Huang X, Garcia-Manero G, Ravandi F, Cortes J, et al. Survival
563 advantage with decitabine versus intensive chemotherapy in patients with higher risk
564 myelodysplastic syndrome: comparison with historical experience. Cancer. 2007;109(6):1133-7.
565 19. Helbig G, Chromik K, Woźniczka K, Kopińska AJ, Boral K, Dworaczek M, et al. Real Life Data
566 on Efficacy and Safety of Azacitidine Therapy for Myelodysplastic Syndrome, Chronic

567 Myelomonocytic Leukemia and Acute Myeloid Leukemia. Pathology & Oncology Research.
568 2019;25(3):1175-80.
569 20. Stahl M, DeVeaux M, Montesinos P, Itzykson R, Ritchie EK, Sekeres MA, et al.
570 Hypomethylating agents in relapsed and refractory AML: outcomes and their predictors in a large
571 international patient cohort. Blood Adv. 2018;2(8):923-32.
572 21. DiNardo CD, Pratz K, Pullarkat V, Jonas BA, Arellano M, Becker PS, et al. Venetoclax
573 combined with decitabine or azacitidine in treatment-naive, elderly patients with acute myeloid
574 leukemia. Blood. 2019;133(1):7-17.
575 22. DiNardo CD, Jonas BA, Pullarkat V, Thirman MJ, Garcia JS, Wei AH, et al. Azacitidine and
576 Venetoclax in Previously Untreated Acute Myeloid Leukemia. New England Journal of Medicine.
577 2020;383(7):617-29.
578 23. Clark SJ, Argelaguet R, Kapourani CA, Stubbs TM, Lee HJ, Alda-Catalinas C, et al. scNMT-seq
579 enables joint profiling of chromatin accessibility DNA methylation and transcription in single cells.
580 Nature Communications. 2018;9(1):781.
581 24. Hunt KV, Burnard SM, Roper EA, Bond DR, Dun MD, Verrills NM, et al. scTEM-seq: Single-cell
582 analysis of transposable element methylation to link global epigenetic heterogeneity with
583 transcriptional programs. Scientific Reports. 2022;12(1).
584 25. Hunt KV BS, Bond DR, Lee HJ. Protocol for targeted analysis of transposable element
585 methylation levels and transcriptome in single cells using scTEM-seq. ProtocolExchange. 2022.
586 26. McCarthy DJ, Campbell KR, Lun ATL, Wills QF. Scater: pre-processing, quality control,
587 normalization and visualization of single-cell RNA-seq data in R. Bioinformatics. 2017;33(8):1179-86.
588 27. Rohart F, Gautier B, Singh A, Le Cao KA. mixOmics: An R package for 'omics feature selection
589 and multiple data integration. PLoS Comput Biol. 2017;13(11):e1005752.
590 28. Rohart F, Eslami A, Matigian N, Bougeard S, Lê Cao K-A. MINT: a multivariate integrative
591 method to identify reproducible molecular signatures across independent experiments and
592 platforms. BMC Bioinformatics. 2017;18(1):128.

593 29. Wickham H. ggplot2: Elegant Graphics for Data Analysis: Springer-Verlag New York; 2016.
594 30. Wu T, Hu E, Xu S, Chen M, Guo P, Dai Z, et al. clusterProfiler 4.0: A universal enrichment tool
595 for interpreting omics data. The Innovation. 2021;2(3):100141.
596 31. Lee EM, Yee D, Busfield SJ, McManus JF, Cummings N, Vairo G, et al. Efficacy of an Fc-
597 modified anti-CD123 antibody (CSL362) combined with chemotherapy in xenograft models of acute
598 myelogenous leukemia in immunodeficient mice. Haematologica. 2015;100(7):914-26.
599 32. Deniz Ö, Ahmed M, Todd CD, Rio-Machin A, Dawson MA, Branco MR. Endogenous
600 retroviruses are a source of enhancers with oncogenic potential in acute myeloid leukaemia. Nature
601 Communications. 2020;11(1):3506.
602 33. Tsai HC, Li H, Van Neste L, Cai Y, Robert C, Rassool FV, et al. Transient low doses of DNA-
603 demethylating agents exert durable antitumor effects on hematological and epithelial tumor cells.
604 Cancer Cell. 2012;21(3):430-46.
605 34. Huang B, Song B-l, Xu C. Cholesterol metabolism in cancer: mechanisms and therapeutic
606 opportunities. Nature Metabolism. 2020;2(2):132-41.
607 35. Duan Y, Gong K, Xu S, Zhang F, Meng X, Han J. Regulation of cholesterol homeostasis in
608 health and diseases: from mechanisms to targeted therapeutics. Signal Transduction and Targeted
609 Therapy. 2022;7(1):265.
610 36. Teramoto T, Watkins C. Review of efficacy of rosuvastatin 5 mg. Int J Clin Pract.
611 2005;59(1):92-101.
612 37. Takeshima H, Yoda Y, Wakabayashi M, Hattori N, Yamashita S, Ushijima T. Low-dose DNA
613 demethylating therapy induces reprogramming of diverse cancer-related pathways at the single-cell
614 level. Clinical Epigenetics. 2020;12(1):142.
615 38. Griffin GK, Wu J, Iracheta-Vellve A, Patti JC, Hsu J, Davis T, et al. Epigenetic silencing by
616 SETDB1 suppresses tumour intrinsic immunogenicity. Nature. 2021.

617 39. Irwin R, Scullion C, Thursby S, Sun M, Thakur A, Rothbart S, et al. UHRF1 suppresses viral
618 mimicry through both DNA methylation-dependent and -independent mechanisms. bioRxiv.
619 2020:2020.08.31.274894.
620 40. Unnikrishnan A, Vo ANQ, Pickford R, Raftery MJ, Nunez AC, Verma A, et al. AZA-MS: a novel
621 multiparameter mass spectrometry method to determine the intracellular dynamics of azacitidine
622 therapy in vivo. Leukemia. 2018;32(4):900-10.
623 41. Yang AS, Doshi KD, Choi SW, Mason JB, Mannari RK, Gharybian V, et al. DNA methylation
624 changes after 5-aza-2'-deoxycytidine therapy in patients with leukemia. Cancer Res.
625 2006;66(10):5495-503.
626 42. Greve G, Andrieux G, Schlosser P, Blagitko-Dorfs N, Rehman U-U, Ma T, et al. In vivo kinetics
627 of early, non-random methylome and transcriptome changes induced by DNA-hypomethylating
628 treatment in primary AML blasts. Leukemia. 2023;37(5):1018-27.
629 43. Li S, Chen X, Wang J, Meydan C, Glass JL, Shih AH, et al. Somatic Mutations Drive Specific, but
630 Reversible, Epigenetic Heterogeneity States in AML. Cancer Discovery. 2020;10(12):1934-49.
631 44. Aumer T, Gremmelmaier CB, Runtsch LS, Pforr JC, Yeşiltaç GN, Kaiser S, et al. Comprehensive
632 comparison between azacytidine and decitabine treatment in an acute myeloid leukemia cell line.
633 Clinical Epigenetics. 2022;14(1):113.
634 45. Flotho C, Claus R, Batz C, Schneider M, Sandrock I, Ihde S, et al. The DNA methyltransferase
635 inhibitors azacitidine, decitabine and zebularine exert differential effects on cancer gene expression
636 in acute myeloid leukemia cells. Leukemia. 2009;23(6):1019-28.
637 46. Li LH, Olin EJ, Buskirk HH, Reineke LM. Cytotoxicity and mode of action of 5-azacytidine on
638 L1210 leukemia. Cancer Res. 1970;30(11):2760-9.
639 47. Vitols S, Norgren S, Juliusson G, Tatidis L, Luthman H. Multilevel regulation of low-density
640 lipoprotein receptor and 3-hydroxy- 3-methylglutaryl coenzyme A reductase gene expression in
641 normal and leukemic cells. Blood. 1994;84(8):2689-98.

642 48. Chiarella E, Nisticò C, Di Vito A, Morrone HL, Mesuraca M. Targeting of Mevalonate-
643 Isoprenoid Pathway in Acute Myeloid Leukemia Cells by Bisphosphonate Drugs. Biomedicines.
644 2022;10(5).
645 49. Banker DE, Mayer SJ, Li HY, Willman CL, Appelbaum FR, Zager RA. Cholesterol synthesis and
646 import contribute to protective cholesterol increments in acute myeloid leukemia cells. Blood.
647 2004;104(6):1816-24.
648 50. Bai S, Wang H, Shao R, Fu B, Lu S, Wang J, et al. Lipid profile as a novel prognostic predictor
649 for patients with acute myeloid leukemia. Frontiers in Oncology. 2023;13.
650 51. Yabushita T, Chinen T, Nishiyama A, Asada S, Shimura R, Isobe T, et al. Mitotic perturbation
651 is a key mechanism of action of decitabine in myeloid tumor treatment. Cell Reports.
652 2023;42(9):113098.
653 52. Dimitroulakos J, Nohynek D, Backway KL, Medley DW, Yeger H, Freedman MH, et al.
654 Increased Sensitivity of Acute Myeloid Leukemias to Lovastatin-Induced Apoptosis: A Potential
655 Therapeutic Approach. Blood. 1999;93(4):1308-18.
656 53. Li HY, Appelbaum FR, Willman CL, Zager RA, Banker DE. Cholesterol-modulating agents kill
657 acute myeloid leukemia cells and sensitize them to therapeutics by blocking adaptive cholesterol
658 responses. Blood. 2003;101(9):3628-34.
659 54. Afzal A, Fiala MA, Jacoby MA, Walter MJ. Statin use in myelodysplastic syndromes is
660 associated with a better survival and decreased progression to leukemia. Blood Advances.
661 2023;7(15):3838-41.
662 55. Brem EA, O'Brien SM, Becker PS, Jeyakumar D, Pinter-Brown LC, Kirk C, et al. A Phase 1 Study
663 of Adding Pitavastatin to Venetoclax-Based Therapy in AML and CLL/SLL. Blood.
664 2023;142(Supplement 1):5940-.

665

Acknowledgements

Nicole Cole (University of Newcastle) provided technical support for fluorescence activated cell sorting. Al J. Abadi (Melbourne Integrative Genomics, University of Melbourne) assisted with the implementation of sPLS analysis. The authors thank Professor Tri Phan (Garvan Institute) and Professor Xu Dong Zhang (University of Newcastle) for critically reviewing this manuscript.

H.J.L., C.R. and M.D.D. received funding from the National Health and Medical Research Council of Australia (NHMRC) (GNT1143614, GNT1180782, GNT1173892, and GNT2016283). K.A.L.C. and H.J.L. received funding from the Australian Research Council (ARC) (DP200102903). H.J.L. and H.C.M. received funding from the Cancer Institute NSW (2018/ECF001 and ECF1299, respectively). D.R.B received funding from Cure Cancer Australia Foundation (CCAF2023-Bond) and NSW Health Pathology North. N.A.B. received funding from the McGuigan family through the Hunter Medical Research Institute (HMRI778). The contents of the published material are solely the responsibility of the research institutions involved or individual authors, and do not reflect the views of funding agencies.

Author Contributions

H.J.L. conceived and oversaw the project. D.R.B., A.K.E., C.R., K.A.L.C., and H.J.L. acquired funding. D.R.B., K.U., K.V.H., B.H., C.L.O., E.A.R., S.H., L.S.R., H.M., and H.J.L. performed experiments. D.R.B., S.M.B., K.U., K.V.H., B.H., C.L.O., L.S.R., C.R., and H.J.L. performed data analysis. S.M.B. and C.R. developed analytical approaches. S.M.B. managed sequencing data and analysis code. D.R.B., N.A.B., A.K.E, N.M.V., K.A.L.C., and H.J.L. supervised work. A.M., M.D.D. and C.E.d.B. provided critical resources. D.R.B., S.M.B., K.U., B.H., L.S.R., C.R., and H.J.L. prepared figures and wrote the manuscript. All authors have read and approved the manuscript.

Ethics Declarations

All experimental procedures using animals were reviewed, approved, and performed according to the Animal Care and Ethics Committee of the University of Newcastle (approval number: A-2023-303), and with consideration of the ARRIVE guidelines (Supplementary Information).

Figure Legends

Figure 1. HMA treatment induces DNA methylation heterogeneity in AML cells. HL-60, MOLM-13 and MV-4-11 cells were labelled with CellTrace and treated with decitabine (DAC; 100nM) or azacytidine (AZA; HL-60: 2000nM, MOLM-13 and MV-4-11: 500nM) every 24h for 72h. Single cells collected by indexed FACS were subjected to scNMT-seq (HL-60) or scTEM-seq (MOLM-13, MV-4-11). **A)** Violin plots of DNA methylation levels in single HL-60 (left), MOLM-13 (middle) and MV-4-11 (right) cells. Superimposed points show single-cell values from untreated (UNT, orange), DAC (cyan) and AZA (purple) groups. Dashed boxes surround DAC and AZA cells with methylation levels within the range of UNT samples. Data are shown for 185-222 cells collected from 2-3 replicate experiments in each cell line (UNT, *n = 27-38*; DAC *n = 63-93*; AZA *n = 68-91*). **B)** Scatter plots comparing CellTrace fluorescence and DNA methylation in single cells, with linear regressions, F-test *p*-values, and Pearson correlation coefficients (*r*). **C)** Violin plots of DNA methylation levels in different genomic contexts from HL-60 scNMT-seq data. **D)** Violin plots of DNA methylation heterogeneity, as determined by pairwise dissimilarity analysis, within different genomic contexts from HL-60 scNMT-seq data. **E)** Box and whisker plots of Pearson correlation coefficients computed within single cells from HL-60 scNMT-seq data. DNA methylation and DNA accessibility were considered in different genomic contexts, and individual loci were matched based on genomic co-ordinates. Correlations were performed between DNA methylation and DNA accessibility (top), DNA methylation and gene expression (middle), and DNA accessibility and gene expression (bottom). Boxes depict the interquartile range (IQR) with median. Whiskers extend to the highest and lowest data points within 1.5 x IQR of the first and third quartile. Outlying data points are not shown.

713 Statistical analysis was performed using ordinary one-way ANOVA with Dunnett's (A) or Šídák's (C-E)
714 multiple comparisons test: * $p < 0.05$, ** $p < 0.0005$ vs. UNT.

715 **Figure 2. HMA-induced epigenetic heterogeneity influences transcriptional programs in AML cells.**
716 HMA treated (AZA and DAC only) HL-60 scNMT-seq data underwent multivariate feature selection by
717 sparse least squares (sPLS) using an unsupervised model. **A)** sPLS projection of cells based on
718 transcript features coloured by cell group 1-4 (from B). **B)** Heatmap of transcript features selected by
719 sPLS displaying all samples (treated and untreated) as columns, are split by k-means clustering and
720 grouped by treatment. Individual gene and TE expression levels (rows) are z-score normalised and
721 split by k-means clustering with internal hierarchical clustering. **C-D)** sPLS projections of cells based
722 on transcript features are coloured by **C)** LINE:L2:L2a expression, and **D)** global methylation level. **E-**
723 **F)** Tree plots of the gene ontology (GO) over-representation analysis (ORA) for gene expression
724 clusters 3 and 1. **G)** Heatmaps summarising the DNA methylation and DNA accessibility features
725 selected by sPLS. Samples (columns) are ordered according to the heatmap in B. The average
726 methylation or accessibility of all sPLS selected features across all samples (treated and untreated) is
727 displayed on the left for each genomic context. The two heatmaps show z-score normalised
728 averages of DNA methylation and accessibility for all sPLS selected features in each genomic context.
729 **H)** Pearson correlations were computed between gene expression and DNA methylation (top) or
730 accessibility (bottom) of associated promoters. Bar graphs show the percentage of correlations ($p <$
731 0.05) with negative (left) and positive (right) coefficients for all genes and filtered by gene expression
732 cluster (identified in D). **I)** Correlations between *RHEX* expression and DNA methylation of adjacent
733 loci (top) are displayed together with annotated short and long interspersed nuclear elements (SINE,
734 LINE), long terminal repeat (LTR), DNA, and Simple repeat sequences (bottom). The blue shading
735 highlights a promoter-proximal region of intron 1 that included 6 regions with negative correlations
736 (cor < -0.3, $p < 0.05$) between DNA methylation and *RHEX* expression.

737 **Figure 3. Highly methylated AML cells display a growth and survival advantage following**
738 **treatment with DAC, but not AZA. A)** HL-60, MOLM-13, and MV-4-11 colony counts following
739 treatment with DAC (cyan) or AZA (purple) vs. untreated cells (UNT, orange). **B-C)** Density plots show
740 the average DNA methylation levels for single cells collected on experiment day 3 (dashed line) and
741 individual colonies collected on experiment day 17 (solid fill) following treatment with DAC or AZA.
742 HL-60 scNMT-seq data were filtered for cytosines within SINE Alu sites for direct comparison to
743 scTEM-seq data from colonies. Data are shown for 288 colonies collected from triplicate
744 experiments in each cell line (*n = 96* per treatment). **D)** Time-course experiment showing changes in
745 average DNA methylation of cells collected at different time points throughout the colony-forming
746 assay (experiment days 6, 10 and 17). Values for experiment day 3 were obtained from single-cell
747 data (Fig. 1A). Data in A and D are expressed as mean +/- standard error of the mean (SEM).
748 Statistical analysis of colony counts (A) was performed using ordinary one-way ANOVA with
749 Dunnett's multiple comparisons test with a $p < 0.05$ cut-off for significance ($p < 0.03$*, $p < 0.006$**, p
750 < 0.0002***).

751 **Figure 4. HMA treatment has sustained transcriptional effects in both methylation-retaining and**
752 **hypomethylated cells. A)** Principal Component Analysis (PCA) plots of single-colony RNA-seq data
753 from AML cell lines, highlighting treatment groups (UNT = orange; DAC = cyan; AZA = purple) and
754 matched mean DNA methylation levels (circle: high > 75%; triangle: low < 75%). Data shown for 119 -
755 220 colonies collected from 3 replicate experiments in each cell line (UNT, *n = 14-73*; DAC, *n = 46-78*;
756 AZA, *n = 56-73*). **B)** Heatmap of the top 2000 highly variable genes from colony RNA-seq data.
757 Samples are ordered by decreasing global methylation levels (green gradient) within each treatment
758 group. Rows are grouped by K-means clusters based on gene expression, with hierarchical clustering
759 by Euclidean distance within each cluster. **C)** GO analysis of the clusters from the top 2000 highly
760 variable genes from B. The size of the circles indicates the gene ratio (number of genes from the
761 input list annotated to the GO term divided by the total number of genes in the input list), and the

762 color represents the significance of the adjusted *p*-value. Gene clusters are color-coded on the y-axis
763 and GO processes are shown on the x-axis.

764 **Figure 5. Altered cholesterol regulation in cells surviving HMA therapy can be targeted to enhance**
765 **treatment efficacy. A)** Box and whisker plots of relative expression for *SREBF1*, *PMVK*, *MVD* and *LSS*
766 in HL-60 (left), MOLM-13 (middle) and MV-4-11 (right) colony data from Figure 5. Pairwise Wilcoxon
767 test between treatment groups was performed with UNT samples as the reference group, for genes
768 present within 'cholesterol biosynthetic process' (GO:0006695). Boxes depict the interquartile range
769 (IQR) with median. Whiskers extend to the highest and lowest data points within 1.5 x IQR of the
770 first and third quartile. Benjamini-Hochberg false discover rate (FDR) correction was performed on
771 all p-values, per cell line: FDR < 0.05*, FDR < 0.01**, FDR < 0.001***. **B)** Colony counts for HL-60
772 (top), MOLM-13 (middle) and MV-4-11 (bottom) cell lines obtained following HMA and rosuvastatin
773 co-treatments. Data from No HMA (orange), DAC (cyan) and AZA (purple) groups are normalised to
774 the corresponding 0 µM rosuvastatin control. Means ± SEM for *n = 3* experiments. Significance
775 determined by two-way ordinary ANOVA with Dunnett's multiple comparisons test, *p* < 0.05* vs.
776 corresponding 0 µM rosuvastatin control. **C)** DNA methylation of colonies formed following DAC and
777 rosuvastatin co-treatments. Means ± SEM for *n = 3* experiments. Significance determined by one-
778 way ANOVA with Tukey's multiple comparisons test, *p* < 0.05* vs. corresponding 0 µM rosuvastatin
779 control.

780 **Figure 6. HMA and statin co-treatment increases survival *in vivo*. A)** Rosuvastatin dose optimisation
781 experiment showing median survival of mice engrafted with MOLM-13-luc cells following treatment
782 with DAC (0.2mg/kg/day) +/- rosuvastatin (1, 10, 40mg/kg/day) on a treatment schedule of '5 days
783 on, 2 days off' for 3 cycles. **B)** Validation of survival benefit when DAC (0.2mg/kg/day) is combined
784 with rosuvastatin (1mg/kg/day) in mice engrafted with MOLM-13-luc AML cells. **C)** AZA and
785 rosuvastatin co-treatment significantly extended median survival of NSG mice engrafted with a
786 patient-derived xenograft (AML-16 model). Mice were treated with AZA (1mg/kg/day) +/-

787 rosuvastatin (1mg/kg/day) for 5 days on, 2 days off in cycle 1, followed by twice per week for an

788 additional 2 cycles. **D)** Leukemia burden (% human $CD45^+$ cells) post-engraftment and following the

789 cessation of treatment. Mann-Whitney test (unpaired, non-parametric, two-tailed t-test) was used

790 to test for statistical significance. Survival analyses (A-C) were performed using Kaplan-Meier

791 analysis followed by the Log-rank (Mantel-Cox) test and an adjusted *p*-value of < 0.05 was

792 considered statistically significant. $p < 0.05$*, $p < 0.005$**, $p < 0.0001$***.

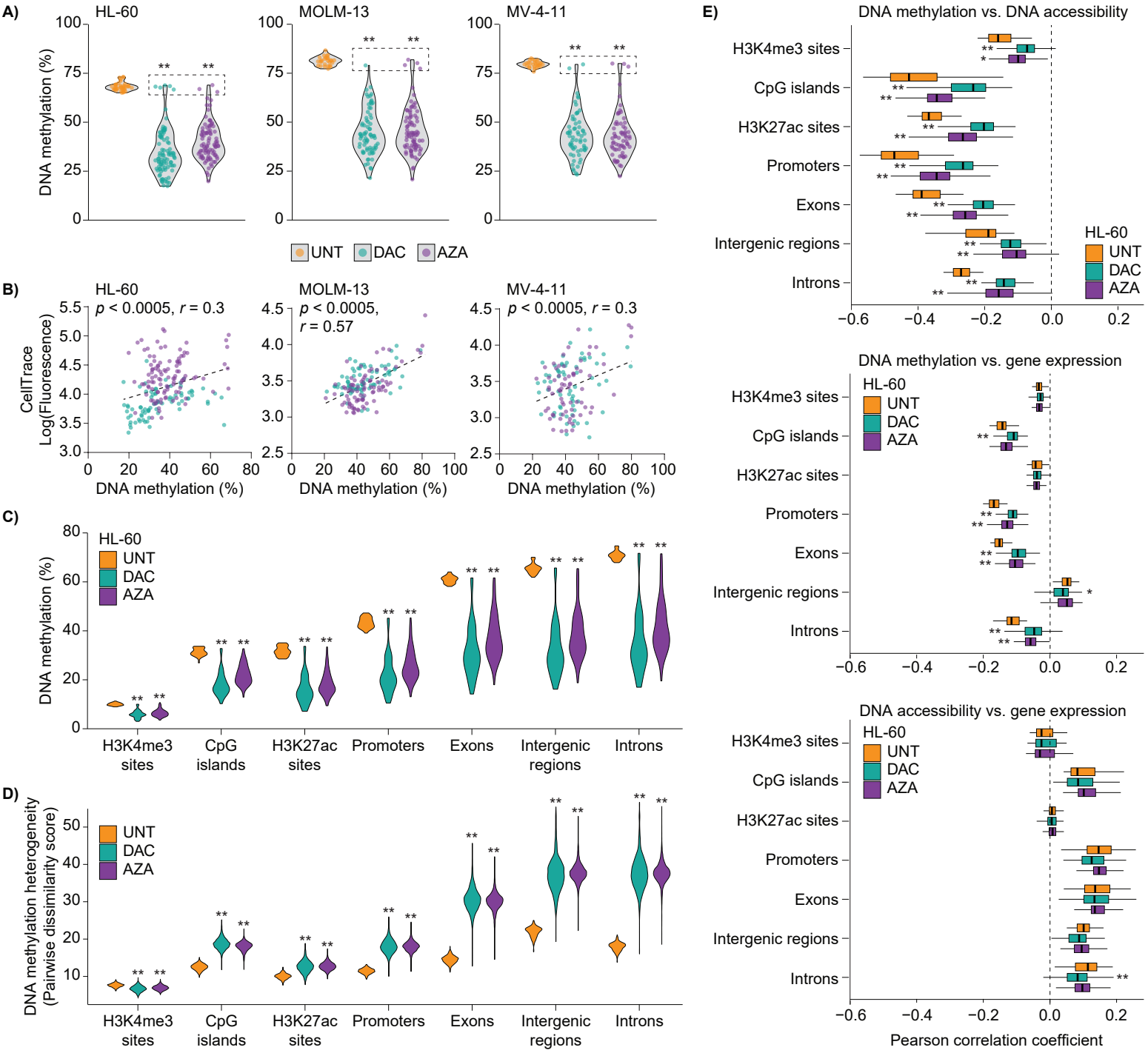
A)
HL-60
MOLM-13
MV-4-11
DNA methylation (%)
UNT
DAC
AZA
B)
HL-60
p < 0.0005, r = 0.3
MOLM-13
p < 0.0005, r = 0.57
MV-4-11
p < 0.0005, r = 0.3
CellTrace Log(Fluorescence)
DNA methylation (%)
C)
HL-60
UNT
DAC
AZA
DNA methylation (%)
H3K4me3 sites
CpG islands
H3K27ac sites
Promoters
Exons
Intergenic regions
Introns
D)
UNT
DAC
AZA
DNA methylation heterogeneity (Pairwise dissimilarity score)
H3K4me3 sites
CpG islands
H3K27ac sites
Promoters
Exons
Intergenic regions
Introns
E)
DNA methylation vs. DNA accessibility
HL-60
UNT
DAC
AZA
DNA methylation vs. gene expression
HL-60
UNT
DAC
AZA
DNA accessibility vs. gene expression
HL-60
UNT
DAC
AZA
H3K4me3 sites
CpG islands
H3K27ac sites
Promoters
Exons
Intergenic regions
Introns
Pearson correlation coefficient

Figure 2

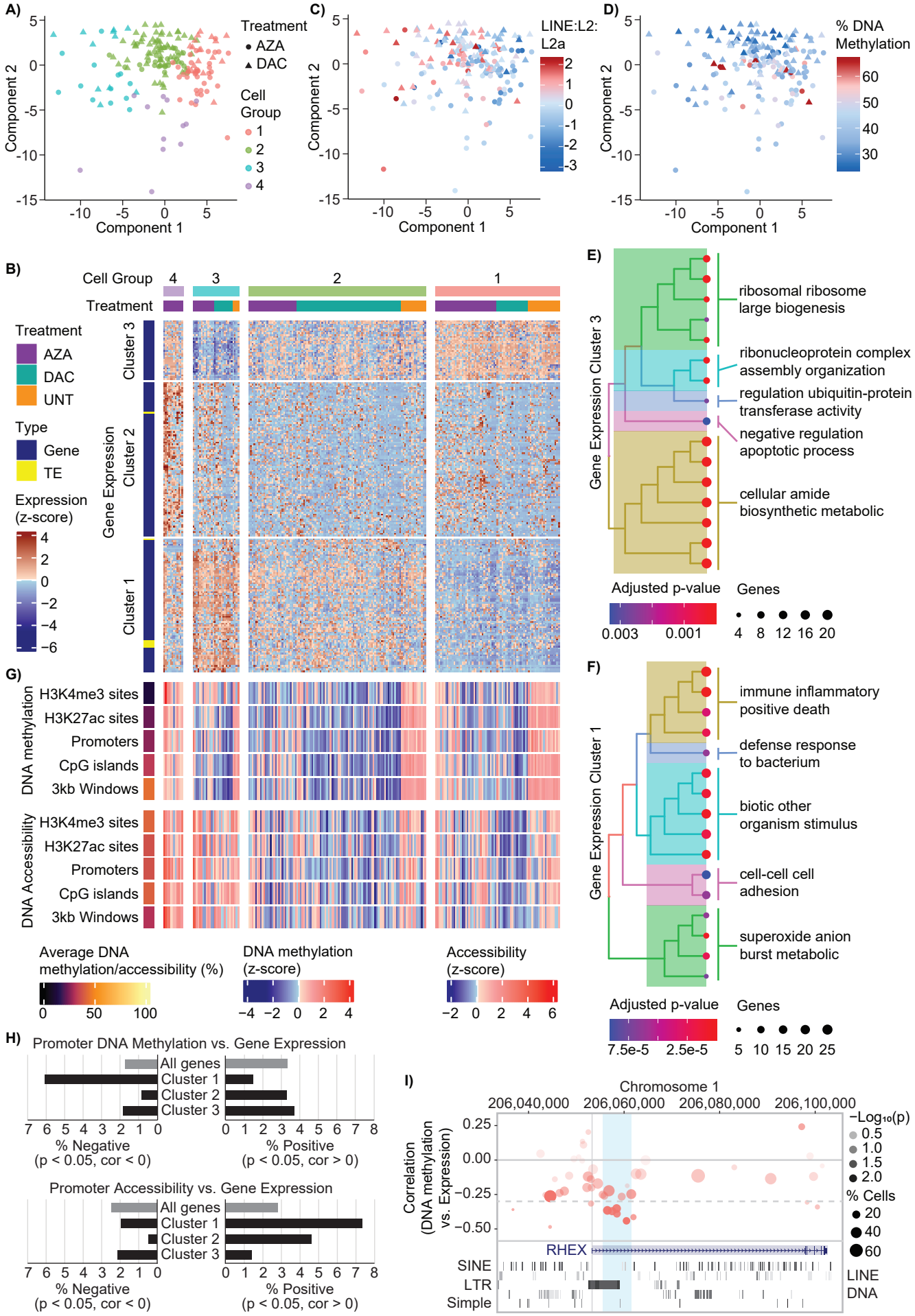
A)
Component 2
Component 1
Treatment
AZA
DAC
Cell Group
1
2
3
4
C)
LINE:L2: L2a
D)
% DNA Methylation
B)
Cell Group
Treatment
Cluster 3
Cluster 2
Cluster 1
Gene Expression
Type
Gene
TE
Expression (z-score)
G)
DNA methylation
H3K4me3 sites
H3K27ac sites
Promoters
CpG islands
3kb Windows
DNA Accessibility
Average DNA methylation/accessibility (%)
DNA methylation (z-score)
Accessibility (z-score)
E)
Gene Expression Cluster 3
ribosomal ribosome large biogenesis
ribonucleoprotein complex assembly organization
regulation ubiquitin-protein transferase activity
negative regulation apoptotic process
cellular amide biosynthetic metabolic
Adjusted p-value
Genes
F)
Gene Expression Cluster 1
immune inflammatory positive death
defense response to bacterium
biotic other organism stimulus
cell-cell cell adhesion
superoxide anion burst metabolic
H)
Promoter DNA Methylation vs. Gene Expression
All genes
Cluster 1
Cluster 2
Cluster 3
% Negative (p < 0.05, cor < 0)
% Positive (p < 0.05, cor > 0)
Promoter Accessibility vs. Gene Expression
I)
Chromosome 1
Correlation (DNA methylation vs. Expression)
−Log10(p)
% Cells
RHEX
SINE
LTR
Simple
LINE
DNA

Figure 3

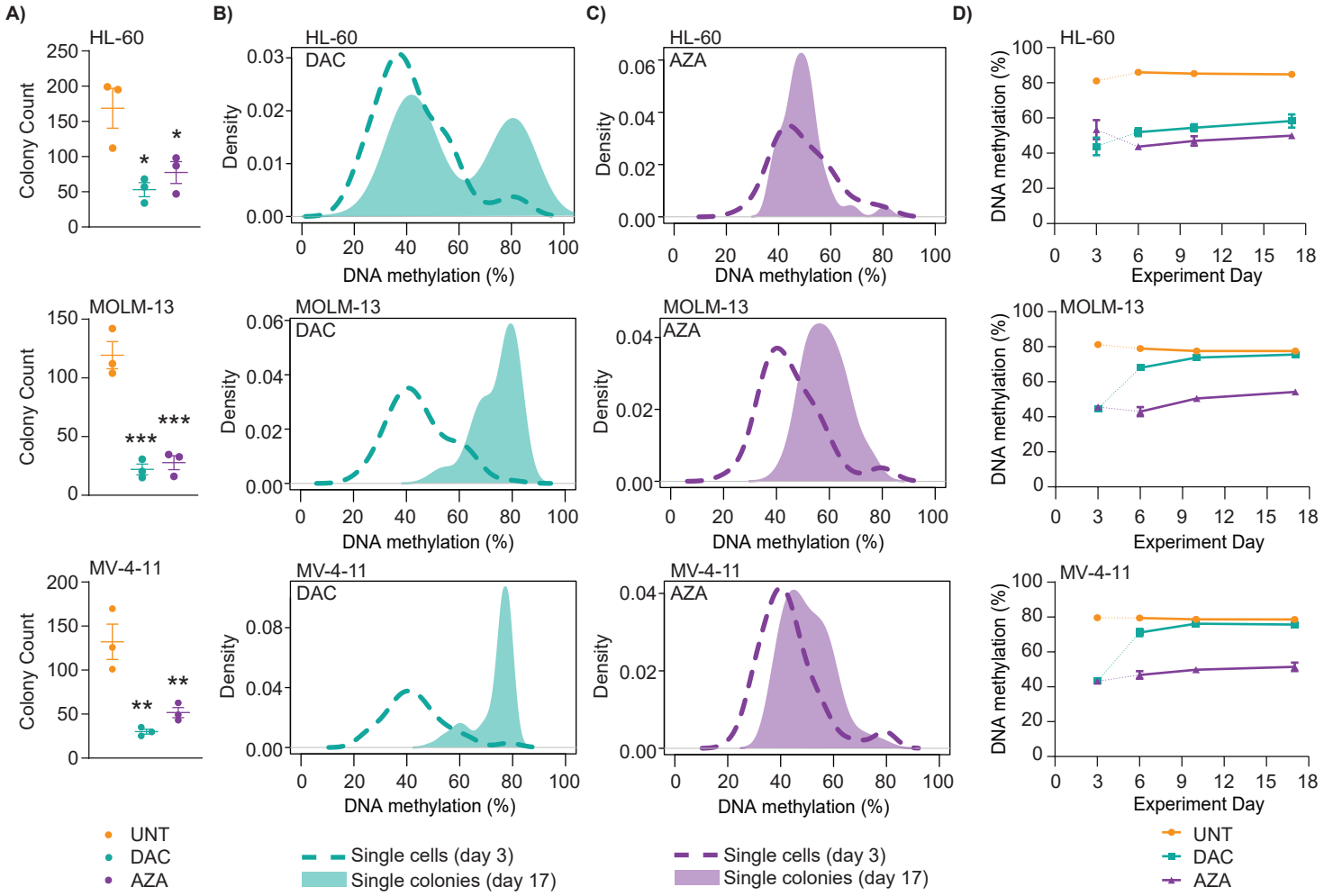
A)
B)
C)
D)
HL-60
MOLM-13
MV-4-11
Colony Count
Density
DAC
AZA
DNA methylation (%)
Experiment Day
UNT
DAC
AZA
Single cells (day 3)
Single colonies (day 17)

Figure 4

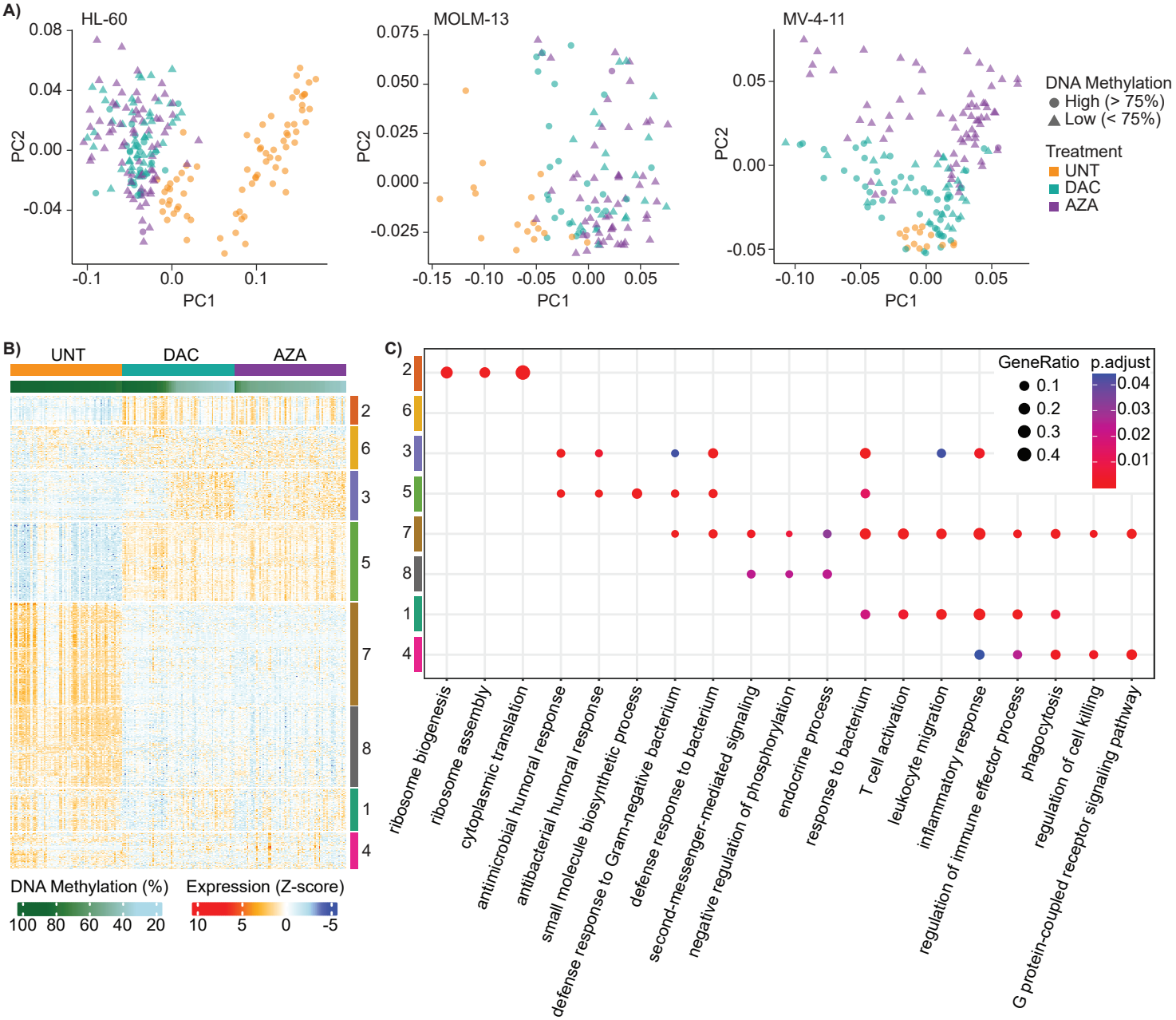
A)
HL-60
MOLM-13
MV-4-11
PC1
PC2
DNA Methylation
High (> 75%)
Low (< 75%)
Treatment
UNT
DAC
AZA
B)
UNT
DAC
AZA
DNA Methylation (%)
Expression (Z-score)
C)
GeneRatio
p.adjust
ribosome biogenesis
ribosome assembly
cytoplasmic translation
antimicrobial humoral response
antibacterial humoral response
small molecule biosynthetic process
defense response to Gram-negative bacterium
defense response to bacterium
second-messenger-mediated signaling
negative regulation of phosphorylation
endocrine process
response to bacterium
T cell activation
leukocyte migration
inflammatory response
regulation of immune effector process
phagocytosis
regulation of cell killing
G protein-coupled receptor signaling pathway

Figure 5

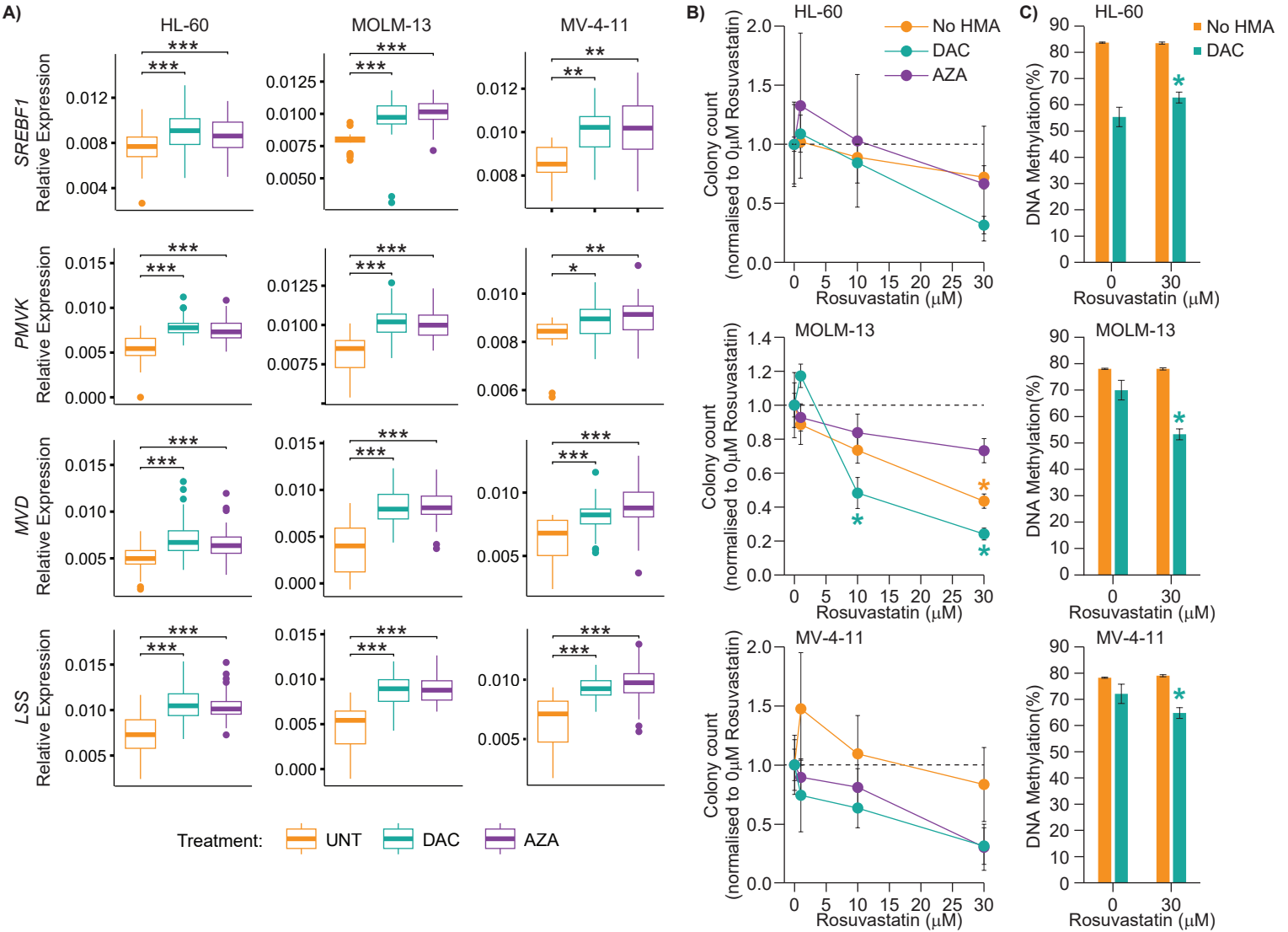
A)
HL-60
MOLM-13
MV-4-11
SREBF1
PMVK
MVD
LSS
Relative Expression
Treatment:
UNT
DAC
AZA
B)
HL-60
MOLM-13
MV-4-11
No HMA
DAC
AZA
Colony count
(normalised to 0μM Rosuvastatin)
Rosuvastatin (μM)
C)
HL-60
MOLM-13
MV-4-11
No HMA
DAC
DNA Methylation(%)
Rosuvastatin (μM)

Figure 6

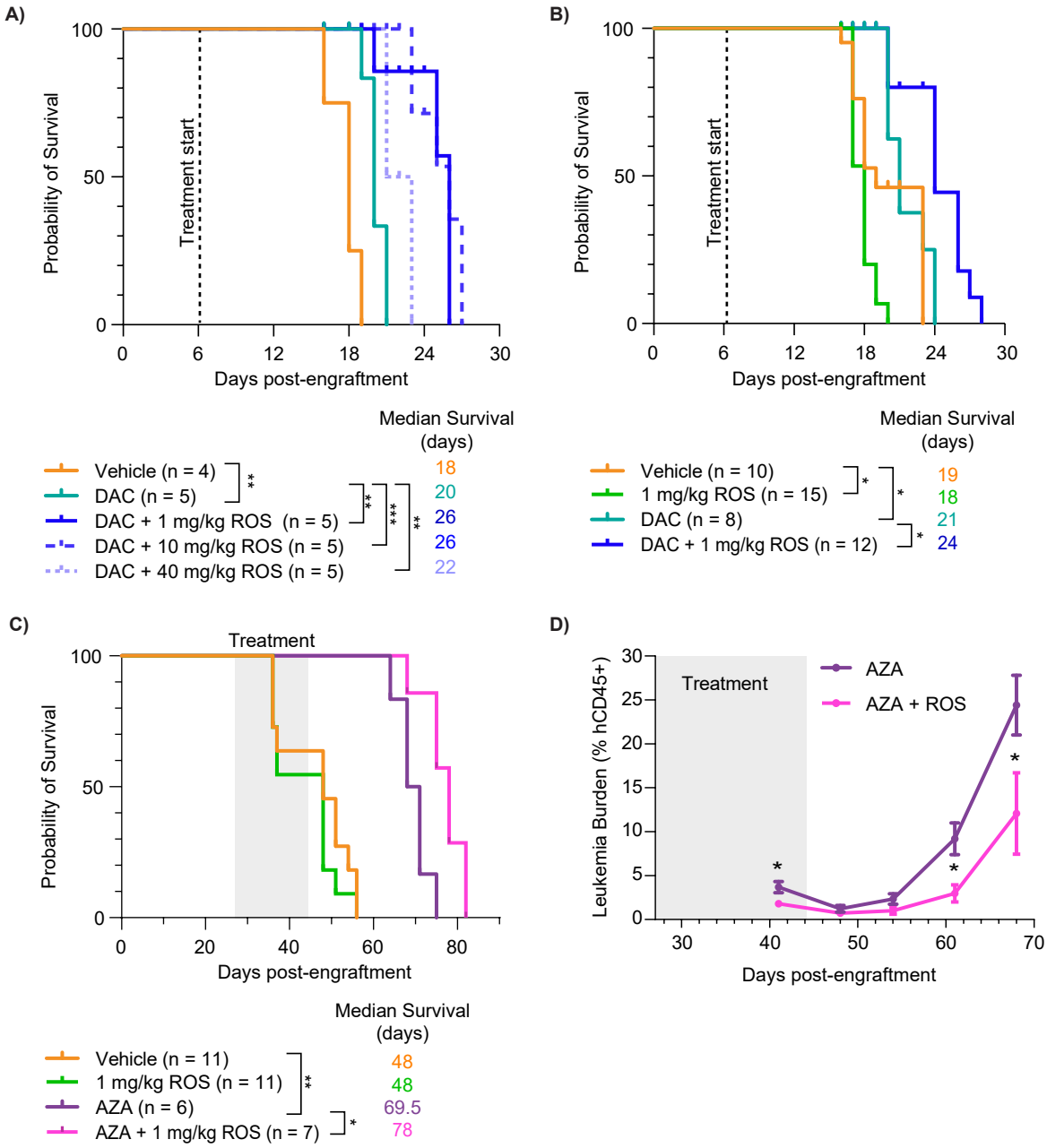
A)
Probability of Survival
Treatment start
Days post-engraftment
Median Survival (days)
Vehicle (n = 4) 18
DAC (n = 5) 20
DAC + 1 mg/kg ROS (n = 5) 26
DAC + 10 mg/kg ROS (n = 5) 26
DAC + 40 mg/kg ROS (n = 5) 22
B)
Probability of Survival
Treatment start
Days post-engraftment
Median Survival (days)
Vehicle (n = 10) 19
1 mg/kg ROS (n = 15) 18
DAC (n = 8) 21
DAC + 1 mg/kg ROS (n = 12) 24
C)
Treatment
Probability of Survival
Days post-engraftment
Median Survival (days)
Vehicle (n = 11) 48
1 mg/kg ROS (n = 11) 48
AZA (n = 6) 69.5
AZA + 1 mg/kg ROS (n = 7) 78
D)
Treatment
AZA
AZA + ROS
Leukemia Burden (% hCD45+)
Days post-engraftment